International Journal of Computer Information Systems and Industrial Management Applications
ISSN 2150-7988 Volume 18 (2026) pp. 1-15

https://doi.org/10.70917/ijcisim-2026-0114
Article

Optimization and Simulation Research on Landscape Design of Lanzhou Waterwheel Based on Three-dimensional Modeling Technology

Lixin Wang *

School of Architecture and Urban Planning, Lanzhou Jiaotong University, Lanzhou, Gangsu, 730070, China; Wlx13919840207@126.com

Abstract: This study proposes a method for the digital reconstruction of the Lanzhou waterwheel landscape based on 3D laser scanning technology. First, point cloud data of the waterwheel surface is obtained through multi-station laser scanning. Public control points are used to align and stitch the point clouds, and feature measure segmentation technology is employed to handle complex scenes. For feature extraction, the AKAZE algorithm is selected to construct a nonlinear scale space, combined with the M-LDB descriptor to enhance rotation and scale invariance. The Flann-based matching process is improved through grid-based preprocessing and group RANSAC model optimization to enhance feature matching accuracy. Based on the point cloud geometric framework, the seed point matching method is employed to achieve precise texture mapping, resulting in a high-fidelity 3D model. Performance validation shows that the model accuracy score in subjective evaluation is 94.85 points, with lighting and shadow effects exceeding 93 points. The AKAZE algorithm reduces skeleton extraction time by 12.1–18.0%. The total modeling time of the model is only 15.24 minutes, which is up to 74.7% faster than the comparison method. The average feature point distance error is 2.33 m, a reduction of more than 57.6%. The spatial stereoscopic level reached 84.12%, significantly higher than the 26.34–63.16% achieved by traditional methods.

Keywords: 3D modeling technology; Lanzhou waterwheel landscape; 3D point cloud technology; AKAZE algorithm; virtual landscape modeling

1. Introduction

Landscape design is a spatial integration activity based on the natural and cultural environment of a specific region, with the aim of preserving cultural diversity [1-2]. As an important highlight of Lanzhou's Yellow River culture and a key node along the Yellow River Scenic Route, waterwheel landscapes play a crucial role in enhancing the city's regional landscape [3]. Therefore, researching human-centered waterwheel landscape design schemes is of great significance for promoting the development of Lanzhou's urban regional landscape with distinct local characteristics.

Given that traditional landscape design methods suffer from issues such as low design efficiency and unpredictable outcomes, the integration of innovative technologies is urgently needed [4-5]. With the continuous development of information technology, digital technology has gradually penetrated all aspects of urban landscape design. Digital technology, particularly 3D modeling technology, has become an essential tool in urban landscape design [6]. The application of 3D modeling technology in landscape design significantly enhances design precision and expressiveness, offering a more intuitive and effective design process than traditional methods [7-9]. In urban landscape design, 3D modeling not only accurately reproduces design concepts but also simulates the actual effects of plants, buildings, water bodies, and terrain, helping designers comprehensively understand spatial relationships and design details [10-12]. Through detailed 3D modeling, designers can clearly present the spatial layout,

vegetation configuration, and functional zoning of the landscape, ensuring that the interactive effects of each design element in the actual site are authentically represented [13-15]. This precise visualization enables designers to better assess the feasibility and effectiveness of the design, providing a basis for subsequent revisions and optimizations [16-17]. Additionally, 3D modeling technology can generate a 360-degree view, allowing designers to observe and adjust design proposals from multiple angles to ensure that the urban landscape achieves the desired effect under different lighting conditions, seasons, and viewpoints [18-20].

With the continuous improvement of computer hardware performance, many scholars have begun to utilize computer-aided design systems to innovate and develop the landscape design process. The application of 3D modeling technology undoubtedly provides strong support for the efficient implementation of landscape design. Jun, Y. and Xian, S. X. discussed the application of digital technology in landscape design and pointed out that a landscape design method integrating projection technology and virtual modeling technology is an optimized strategy suitable for the current state of landscape design in China [21]. Tian, Z. emphasized that modern landscape design requires a dual focus on creativity and technology. With the support of virtual reality technology, powerful three-dimensional modeling and physical rendering processes optimize the landscape design process, enabling continuous improvements before completion [22]. Liu, C. et al. proposed a multi-dimensional urban landscape design method based on nonlinear theory, which, when introduced into the landscape design and planning process in virtual scene spaces, can effectively enhance the visual expression capabilities of urban landscape design, thereby addressing the issue of significant variability in multi-dimensional urban landscape design [23]. Liu, X. introduced virtual modeling technology and three-dimensional visualization technology for urban landscape planning and design. Virtual reality modeling can fully demonstrate the actual effects of drawings to enhance design efficiency and quality, while three-dimensional visualization technology provides professionals with intuitive, rapid detection, and interactive pathways [24]. Lee, M. J. analyzed the role of various digital technologies in landscape architecture drawing, arguing that these technologies should serve as auxiliary tools to facilitate exploration across all aspects of landscape design rather than as replicas of real-world landscapes [25]. Shan, P. and Sun, W. developed a new landscape planning effect simulation system based on virtual reality technology, combining feature enhancement techniques and parametric modeling methods to achieve virtual construction and presentation of landscapes, significantly improving design efficiency [26]. However, the widespread adoption and practical application of these technologies still face certain challenges. How to fully and efficiently apply 3D modeling technology to the landscape design process of the Lanzhou Waterwheel Landscape will be a key research topic for this project.

This study first focuses on the efficient collection and processing of three-dimensional laser scanning point cloud data. For the complex three-dimensional object of a waterwheel, we first employ laser three-dimensional point cloud stereoscopic non-contact measurement technology to obtain the three-dimensional coordinate information of a large number of points on the surface of the waterwheel through multi-station scanning. By identifying common control points, we calculate the precise rotation and translation transformation matrix to achieve point cloud data registration and stitching. Facing the complex point cloud scene composed of the wooden structure of the waterwheel, water body, and surrounding environment, we further employ feature-based point cloud segmentation technology to divide the point cloud data into homogeneous subregions with similar attributes. Based on this, we select the AKAZE algorithm, which has good robustness and efficiency, for image feature point extraction, construct a nonlinear scale space, and determine the principal direction of feature points. We use the M-LDB descriptor to generate feature descriptions with rotation and scale invariance. To address the potential clustering of feature points in waterwheel images and improve matching accuracy, the traditional Flann-based matching combined with the RANSAC screening process was improved by introducing grid-based preprocessing and group-based calculation of model parameters, effectively enhancing the accuracy and reliability of feature point matching and providing precise correspondences for subsequent model texture mapping. Finally, three-dimensional virtual landscape modeling and design were performed. Based on a point cloud-described geometric framework, the landscape's external and internal attributes are analyzed. Texture information is obtained from scanned objects, and texture features are analyzed using the seed point matching method for attribute segmentation. Finally, the two-dimensional texture image is precisely mapped onto the three-dimensional geometric model, completing the construction of a realistic three-dimensional virtual waterwheel landscape model.

2. Digital Reconstruction Method for Lanzhou Waterwheel Landscape Based on 3D Modeling Technology

2.1. 3D Landscape Design Based on Laser 3D Point Cloud Technology

2.1.1. 3D Landscape Data Collection Using Laser 3D Point Cloud Technology

To efficiently collect three-dimensional information about landscapes, laser-based three-dimensional point cloud stereoscopic non-contact measurement technology is employed to obtain the three-dimensional coordinates of data points on the landscape surface. The laser line structured light from the laser 3D scanning device is projected onto the 3D landscape. Based on the line images of the landscape surface captured by the charge-coupled device (CCD) camera, the 3D coordinates of the image points are determined. The scanning mode of the device is as follows: by adjusting the rotation speed of the prism in the rotation device, the corresponding scanning speed is obtained. The landscape is scanned at various vertical scanning angles. Through the circular rotation of the optical surface, the landscape is scanned comprehensively in the horizontal plane.

The coordinate system is a key point in the collection of three-dimensional coordinate information for landscapes, and the transformation between different coordinate systems is particularly important. Figure 1 shows the transformation between different coordinate systems, where M_{SOP} and M_{POP} represent the transformation matrices from the scanning device to the project and from the project to the global coordinate system, respectively, and the superscript -1 indicates the inverse transformation matrix.

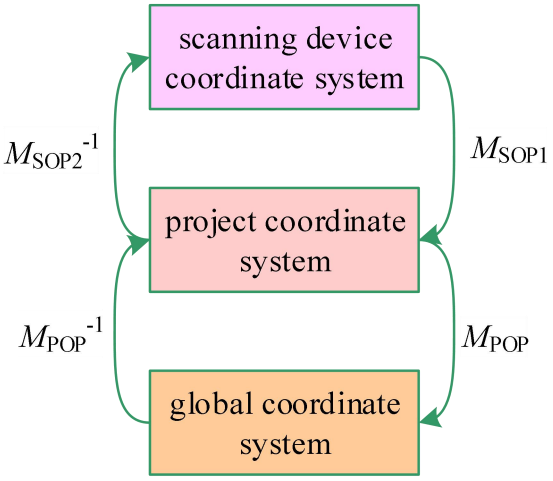

Figure 1. Schematic diagram of the transformation of various coordinate systems.

During the coordinate transformation process, homogeneous coordinates are used to define three-dimensional spatial coordinate points. The transformation matrix is shown below:

$$T_{3D} = \begin{pmatrix} a_{11} & a_{12} & a_{13} & a_{14} \\ a_{21} & a_{22} & a_{23} & a_{24} \\ a_{31} & a_{32} & a_{33} & a_{34} \\ a_{41} & a_{42} & a_{43} & a_{44} \end{pmatrix} \tag{1}$$

The formula consists of four submatrices: $\begin{pmatrix} a_{11} & a_{12} & a_{13} \\ a_{21} & a_{22} & a_{23} \\ a_{31} & a_{32} & a_{33} \end{pmatrix}$, $(a_{41}\ a_{42}\ a_{43})$, $\begin{pmatrix} a_{14} \\ a_{24} \\ a_{34} \end{pmatrix}$, and (a_{44}), which are used for geometric transformation, translation transformation, projection transformation, and overall transformation, respectively.

Only when the laser point cloud data collected from various directions overlap can landscape image stitching be completed. Therefore, based on the solution values of the linear equation system R of the three-dimensional coordinates of any point, the transformation matrix parameters can be determined. Point cloud data is only related to rotation and translation during stitching, so the following equation

applies:

$$\begin{cases} \begin{pmatrix} a_{14} \\ a_{24} \\ a_{34} \end{pmatrix} = \begin{pmatrix} 0 \\ 0 \\ 0 \end{pmatrix} \\ (a_{44}) = (1) \end{cases} \tag{2}$$

In summary, by utilizing four non-collinear common points in different regions, the corresponding transformation matrix can be obtained. Assuming that the rotation parameters and translation parameters of the coordinate system are $r_{11} \sim r_{33}$ and $t_1 \sim t_3$, respectively, the fourth-order rotation-translation matrix that achieves the coordinate system transformation is: $\begin{pmatrix} r_{11} & r_{12} & r_{13} & 0 \\ r_{21} & r_{22} & r_{23} & 0 \\ r_{31} & r_{32} & r_{33} & 0 \\ t_1 & t_2 & t_3 & 1 \end{pmatrix}$.

2.1.2. Point Cloud Data Preprocessing

Each observation point is equipped with three laser scanning stations, and the data collected by the three scanning stations must be aligned and stitched together. Alignment and stitching of point cloud data are achieved by setting up control points with the same name on the landscape surface. Let the corresponding data point sets of measurement data points in the overlapping area from different perspectives be denoted by A and B, respectively. Let the subset $\{m_i \mid m_i \in A, i = 1, 2, \cdots, N\}$ is extracted from the data point set A; the subset $\{m_i' \mid m_i' \in B, i = 1, 2, \cdots, N\}$ is extracted from the data point set A, and the two points correspond to each other. Point cloud registration is achieved by obtaining the translation and rotation coordinate transformation relationships of the data points collected from each perspective. Let G and K denote the translation matrix and rotation matrix, respectively. Point cloud registration essentially involves minimizing the objective function. The objective function satisfying the translation and rotation transformation matrices is established as follows:

$$f(K, G) = \min \sum \left[K \cdot a_i + G - b_i \right] \tag{3}$$

In the formula, a_i and b_i are the collection points that need to be registered.

Laser scanning data was collected using any point as the station. The coordinate systems of each group of point cloud data were not unified. The target of the first station was set as the reference coordinate, and the data collection points of the second and third stations were registered with the first station. The RiSCAN pro software was used to complete the fine registration of the point cloud data.

2.1.3. Point Cloud Segmentation

Three-dimensional landscape scene point cloud data is typically complex. Through point cloud segmentation, complex three-dimensional landscapes can be represented using homogeneous units with similar feature measures. Feature measures include parameters such as average elevation, model fitting parameters, and spectral information obtained from point cloud data acquired by laser scanning technology. A single measure is represented using a high-dimensional feature space vector, and point cloud data is segmented in high-dimensional feature space using clustering segmentation methods. Let P denote the set of scanned points, and let Q denote the surface area associated with the point set P. The set of subregions of Q is denoted by $\{Q_1, Q_2, \cdots, Q_i, \cdots, Q_n\}$. When this set of subregions satisfies the following conditions, it constitutes the regional segmentation of the point set P.

(1) $\bigcup_{i=1}^{n} Q_i = Q$. All points can be partitioned into a certain region, i.e., Q is the union of the partitioned subregions;

(2) $Q_i \bigcap Q_j \neq \phi$, $\forall i \neq j$. Random points cannot belong to different partitioned regions ϕ at the same time, i.e., there is no overlap between partitioned regions;

(3) $Q_i, i = 1, 2, \cdots, n$. Q_i represents a connected region, and the points within each partitioned region are mutually connected;

(4) $L(Q_i) = True$, $i = 1, 2, \cdots, n$. The similarity operator $L(Q_i)$ indicates whether points with the same similarity measure exist within the same partitioned region;

(5) $L(Q_i) = False$, $\forall i = 1, 2, \cdots, n$, $j = 1, 2, \cdots, n$, $i \neq j$. Differences exist Similarity measure characteristics exist in different partition regions.

2.2. Image Feature Point Extraction and Matching

The AKAZE algorithm is selected for image feature point extraction. This algorithm exhibits good robustness and fast feature point extraction rates. The extracted feature points can be reused, ensuring high sustainability. The feature extraction process is as follows:

(1) Image denoising and transfer function determination: Based on the principle of Gaussian filtering, the image is denoised, and the transfer function $c(x, y, t)$ of the image is determined, where (x, y) represents the pixel coordinates of the image, and t represents the evolution time.

(2) Calculation of evolution time:

$$t_i = \frac{1}{2}\sigma_i^2 \tag{4}$$

In equation (4), σ_i is the scale parameter of the original image; i is the image scale.

(3) Brightness matrix update (introduction of the FED algorithm): To ensure the algorithm's operating speed, the FED algorithm is introduced to update the brightness matrix:

$$L^{i+1} = (I + \tau A(L^i))L^i \tag{5}$$

In equation (5), L_i is the brightness matrix of image scale i ; I is the identity matrix; τ is the time step; $A(L^i)$ represents the conduction matrix of L_i .

(4) Introduce a nonlinear partial differential equation to describe the brightness changes in the image:

$$\frac{\partial L}{\partial t} = div(c(x, y, t) \cdot \nabla L) \tag{6}$$

In equation (6), ∂ is the differential symbol; L is the image brightness matrix; $|div$ is the image brightness divergence; t is the evolution time; $c(x, y, t)$ is the conduction function; ∇ denotes the brightness gradient in the $c(x, y, t)$ function.

By iteratively updating equations (5) and (6), the nonlinear scale space is constructed.

(5) Introduce the Hessian matrix:

$$L_{i,\max} = \begin{pmatrix} \frac{\partial^2 L_i}{\partial t_1^2} & \frac{\partial^2 L_i}{\partial t_1 \partial t_2} & \cdots & \frac{\partial^2 L_i}{\partial t_1 \partial t_n} \\ \frac{\partial^2 L_i}{\partial t_1 \partial t_2} & \frac{\partial^2 L_i}{\partial t_2^2} & \cdots & \frac{\partial^2 L_i}{\partial t_2 \partial t_n} \\ \vdots & \vdots & \ddots & \vdots \\ \frac{\partial^2 L_i}{\partial t_n \partial t_1} & \frac{\partial^2 L_i}{\partial t_n \partial t_2} & \cdots & \frac{\partial^2 L_i}{\partial t_n^2} \end{pmatrix} \tag{7}$$

According to equation (7), calculate the extreme values of L_i in different intervals of the image, i.e., determine the feature points of the image. Then, take the feature point a as the center and determine a circular region with a radius of r . Randomly select a six-segment sector region in this circle. calculate the sum of the gradient vectors of the feature points in the sector regions in different directions from point a , denoted as $\vec{a}$, and select the maximum value of $\vec{a}$, denoted as $\vec{a}_{\max}$. The direction of this vector is the principal direction of the feature point.

(6) M-LDB descriptor: Finally, describe using the M-LDB descriptor $\vec{a}_{\max}$ proposed by this

algorithm.

After rotation and scale changes, the M-LDB descriptor does not change the relevant information of the feature points, which is conducive to the matching of feature points between different images.

Select a Flann-based method to match the extracted image feature points. This matching method can obtain more matching feature points. To reduce the impact of incorrectly matched feature points on subsequent work, the matched feature points must be screened to select correctly matched feature points with better feature representation capabilities. Screening is generally performed using the RANSAC algorithm. However, due to the random distribution of feature points in the image, there may be feature point clustering, which can cause the mathematical model constructed by the RANSAC algorithm to exhibit excessive locality and poor local removal effects. To address these issues, the RANSAC algorithm is modified as follows:

First, based on the maximum and minimum values of the horizontal and vertical coordinates of the selected feature points, determine the distribution range $W \times H$ of the feature points and divide it into $a \times b$ unit grids. Next, remove image blocks from grids that do not contain feature points. For grids containing multiple feature points, retain only the feature points with the highest matching scores. Then, randomly group the retained feature points into groups of four. Finally, discard groups with fewer than 4 feature points; then, calculate the image transformation matrix model parameters for each group using the RANSAC algorithm, and record the number of transformation matrix models. If this number is greater than s and less than z, record all transformation matrix models. If this number is less than s, the feature point grouping calculation is performed again.

The values of W and H in the improved algorithm are related to the extracted image feature points. The values of a and b can be adjusted according to the image size and image matching requirements. The optimal values of s and z can be determined through experimentation.

Based on the above analysis, the process of image feature point extraction and matching is shown in Figure 2.

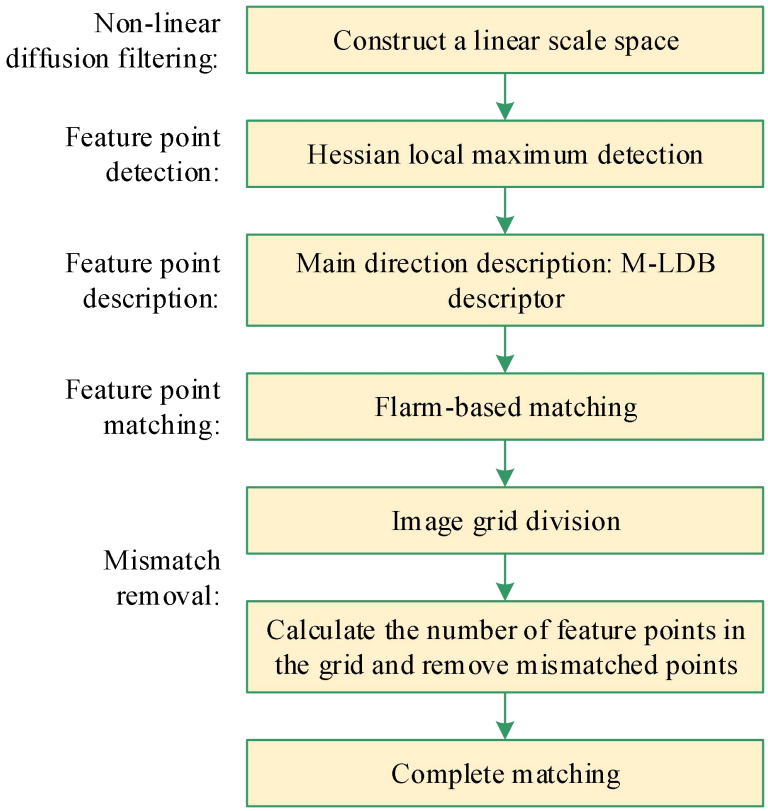

Figure 2. The process of extracting and matching image feature points.

2.3. Modeling and Virtual Design Based on Three-Dimensional Virtual Landscapes

At this point, we have obtained point cloud data describing the precise three-dimensional geometric structure of the Lanzhou waterwheel landscape, as well as texture images characterizing its surface visual features and their corresponding relationships. Based on these core data, we can proceed with the modeling and design of a three-dimensional virtual landscape.

2.3.1. Three-Dimensional Virtual Landscape Modeling—Analysis of Landscape Attributes

Based on the use of dynamic descriptive space to describe the structural characteristics of landscapes, an analysis of the external and internal attributes of landscapes is conducted. The mapping relationship of landscape surface attributes in this analysis process is shown in Figure 3.

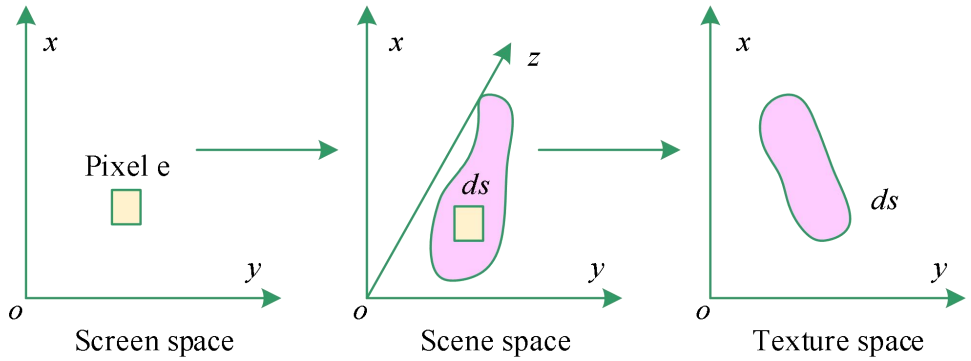

Figure 3. Mapping relationship of landscape appearance attributes.

In the figure: x, y represent the horizontal and vertical coordinates; z represents the spatial dimension; ds, dA represent the mapping surface. Most objects in real-world landscapes have textures on their surfaces. Therefore, when modeling virtual landscapes, it is necessary to consider the color and brightness differences introduced by these textures. A related seed point matching method is used to segment the texture attributes and analyze their features. The computational process is as follows:

$$L = \varphi(j) \cdot f(x, y) - \sum_{i=1}^{n} a_n x_i^2 + b_n y_i^2 + c_n x_i y_i \tag{8}$$

In the equation: $f(x, y)$ represents the iterative feature function of texture changes; x denotes the horizontal coordinate of the texture vector at fixed point i; y denotes the vertical coordinate of the texture vector at fixed point i; a, b, c represent the matching constants between n textures and time, space, and material; $\varphi(j)$ represents the trend direction of object textures in the actual landscape. Using a scanner to perform a characterization scan of physical objects, texture mapping software is used to convert the texture of physical objects into two-dimensional planar graphics. Using feature matching methods, this image is mapped onto the aforementioned landscape geometric models. When rendering object surfaces, attention must be paid to the corresponding object colors. Function textures, such as two-dimensional texture patterns, are then applied as geometric textures for the landscape. At this point, the modeling and construction of the three-dimensional virtual landscape are complete.

2.3.2. Three-Dimensional Virtual Landscape Virtual Design

Based on the completed virtual landscape model, the data in the image is corrected. The created image is uploaded to PHOTOSCOP 9.0 for data preprocessing, then saved in *.tif file format. This file is then uploaded to ERDAS software, where it is saved in *.img format, and the correction process begins. The coordinate correction method consists of two steps: first, select control points using a window image with an actual coordinate system; second, input the actual coordinates of the landscape into the software to perform image correction, resulting in a precise corrected image.

When designing outdoor virtual landscapes based on a 3D landscape model, the triangular point method is used to convert terrain data into digital information. 3D data simulation is employed to construct the virtual terrain of the landscape. The terrain features of the virtual outdoor landscape are

shown in Figure 4.

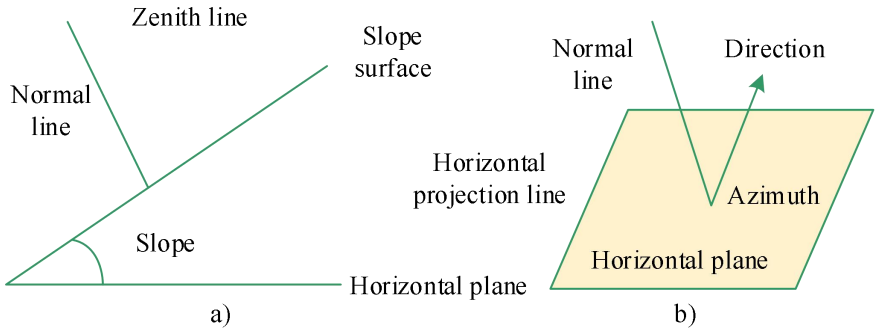

Figure 4. Outdoor landscape terrain slope design.

As shown in Figure 4, based on the grid plane, the slope and slope direction of the landscape design are determined. The angle between the projection of the foot line on the horizontal plane and the actual direction is the slope direction angle, while the slope is the angle between the three-dimensional plane and the horizontal plane. The formula for calculating the slope between two points is:

$$\alpha = \frac{\mu_a - \mu_b}{d_{ab}} \times 100\% \tag{9}$$

In the formula: μ_a represents the contour line value at the highest point a; μ_b represents the contour line value at the lowest point b; d_{ab} represents the horizontal distance between the highest point a and the lowest point b. Next, a virtual design of the indoor landscape is created using the established virtual landscape model to construct the indoor landscape imagery. The indoor and outdoor virtual landscape models are assembled, with the indoor landscape model seamlessly integrated with the outdoor landscape. Adjustments are made based on data such as scale and angle to refine the orientation and arrangement, ultimately constructing the overall three-dimensional form of the virtual landscape.

3. Performance Verification and Comparative Analysis of the Three-Dimensional Modeling Scheme for the Lanzhou Waterwheel Landscape

This paper first uses laser 3D point cloud technology to collect and process relevant data on the Lanzhou Waterwheel Landscape Project. Then, Blender is used to create a 3D model of the landscape data. Finally, Unity3D is used to display the Blender data through virtual reality technology. To verify the practicality of this approach, it is applied to actual landscape simulations for application analysis.

3.1. Convergence Test

First, a convergence test is conducted on the Lanzhou waterwheel landscape model constructed using 3D modeling technology. To determine whether the calculation has converged, a comprehensive assessment must be made. Relying solely on residual value analysis is insufficient to meet all requirements.

In this experiment, convergence testing is performed through residual value monitoring. During each time step of the calculation process, when the residual values of all physical variables meet the convergence criteria, the calculation is considered to have converged. Fluent's default convergence criteria are met when the residual values of all variables drop below 1×10^{-6}, with the convergence criteria for energy residual values set below 1×10^{-3}. The residual values from the verification condition calculations are shown in Figure 5, which meet the convergence criteria.

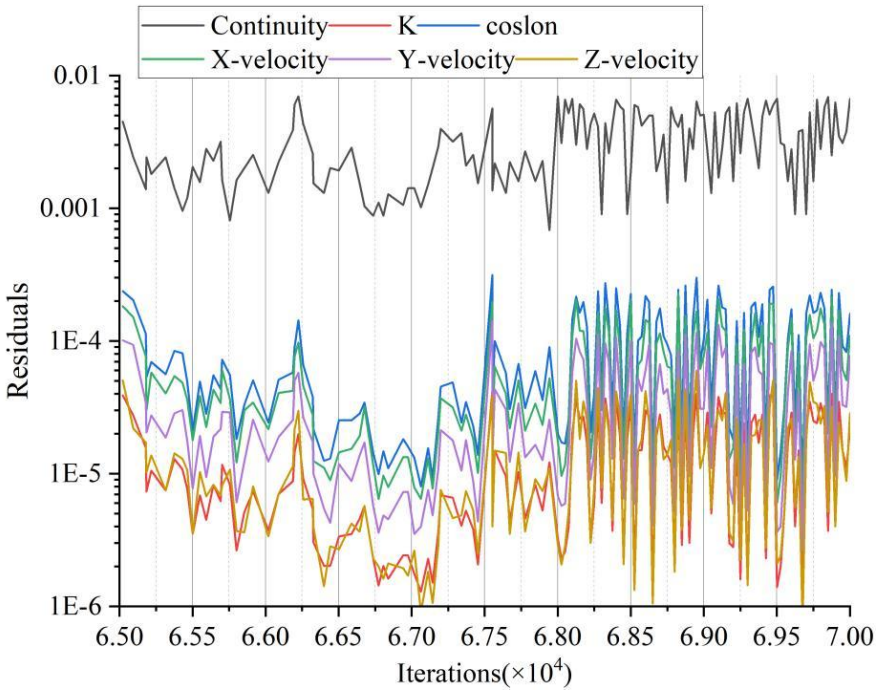

Figure 5. Residual value monitoring window.

3.2. System Evaluation Score

Based on ensuring the convergence of the model, we further recruited volunteers to conduct subjective evaluations of landscape realism and environmental elements, quantifying the model's visual performance from a user perspective.

The experiment recruited 20 volunteers to evaluate the landscape realism and environmental elements presented in the design scheme. The evaluation dimensions were divided into five aspects: model accuracy, materials and textures, resolution, lighting effects, and shadow effects, with a total score of 100 for each dimension. Figure 6 shows the statistical results of the average scores for each indicator under the realism and environmental elements dimensions of the Lanzhou waterwheel landscape scene simulated by the three-dimensional modeling scheme based on laser point cloud data proposed in this paper, as evaluated by the 20 volunteers.

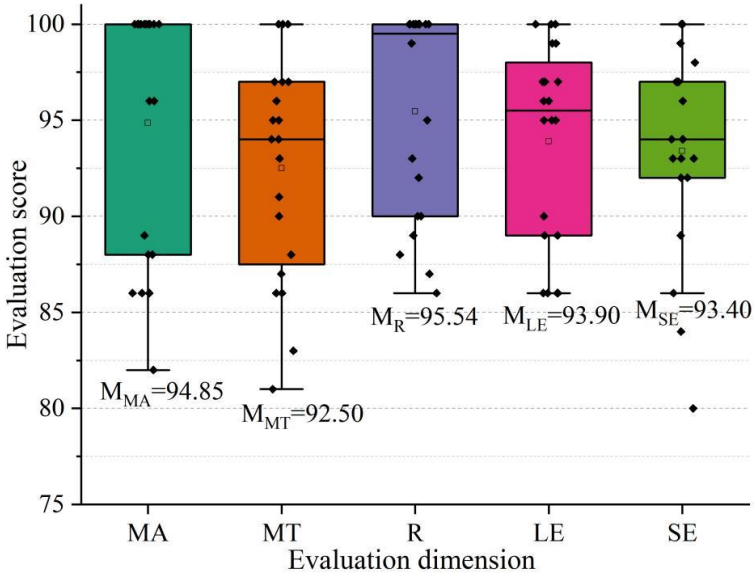

Figure 6. The scores of each evaluation dimension of the system.

In the landscape realism dimension, the model achieved the highest accuracy score, averaging 94.85 points, indicating that the geometric structure reconstructed from point cloud data closely matches the actual form of the waterwheel. The average scores for resolution and material texture were 95.45 and 92.50 points, respectively, indicating that the model's geometric detail reproduction outperforms the authenticity of surface materials. In the environmental elements dimension, both lighting effects (93.90 points) and shadow effects (93.40 points) exceeded 93 points, validating the naturalness of the virtual scene's lighting and shadow simulation. All dimensions scored above 92 points, confirming that this method can accurately reproduce the geometric and visual characteristics of the Lanzhou waterwheel landscape.

3.3. Extraction of the Skeleton and Model Construction of the Lanzhou Waterwheel Landscape Based on Point Cloud Data

In addition to subjective evaluation, objective assessment of modeling efficiency is also required. This section analyzes the performance improvement of large-scale data processing through algorithm optimization based on the time required for point cloud skeleton extraction and mesh reconstruction.

3.3.1. Analysis of Skeleton Generation Results

Table 1 and Figure 7 (visualization) show the average time required to extract skeletons from point cloud data before and after optimization using the AKAZE algorithm for image feature point extraction and matching. It can be seen that optimization reduces the average time required to extract skeletons, and the longer the average time required to extract skeletons before optimization, the more obvious the optimization effect.

Table 1. Comparison of time of skeleton extraction before and after optimization.

Number of point clouds	Import time /ms	The time of extracting the skeleton /ms	
		Before optimization	After optimization
4651	16.9	4.2	3.9
6480	22.5	5.1	4.8
9125	35.6	22.2	20.4
12363	45.2	44.7	40.3
22271	71.7	79.5	65.2
53910	132.5	106.4	94.1
87994	267.3	218.7	183.2
158379	506.9	314.5	276.4

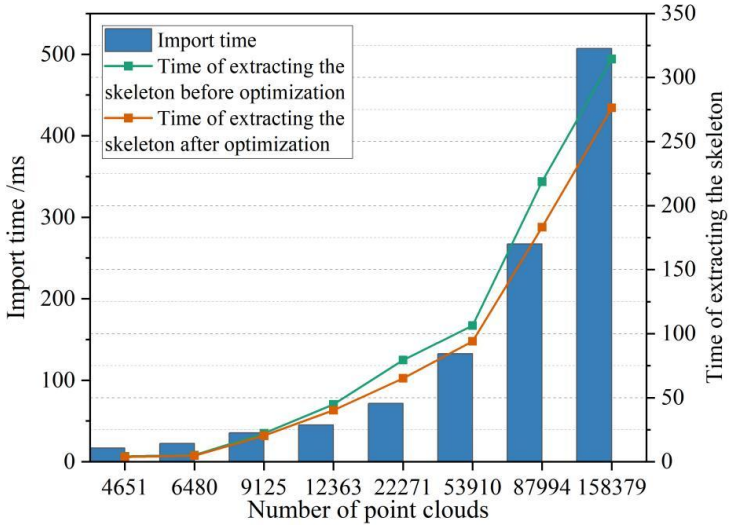

Figure 7. The duration of extracting the skeleton before and after optimization.

As can be clearly seen from the figure, the optimization effect is significant, with the extraction time decreasing for all point cloud sizes, and the optimization becoming more pronounced as the data volume increases. For example, when the point cloud size is 158,379, the processing time decreases from 314.5ms to 276.4ms (a reduction of 12.1%); when the point cloud size is 222,71, the processing time decreases from 79.5ms to 65.2ms (a reduction of 18.0%). The non-linear relationship between scale and processing time is evident: when the point cloud size increased from 46,351 to 158,379, the processing time increased by nearly 75 times before optimization (4.2ms → 314.5ms), and by 71 times after optimization (3.9ms → 276.4ms), indicating that the algorithm optimization effectively mitigates the time expansion issue in large-scale data processing.

3.3.2. Reconstruction of Landscape Grid Model-Related Data

The performance of the landscape system based on point cloud data was further analyzed. Table 2 shows the number of points in some point cloud data, import time, average runtime required to reconstruct the landscape mesh model, and the number of mesh model faces generated.

Table 2. Data related to Landscape mesh model reconstruction.

Number of point clouds	Import time /ms	The running time of the reconstructed landscape grid model /ms	Model facets (10,000 facets)
4651	16.9	2.7	248.17
6480	22.5	3.2	309.63
9125	35.6	0.2	13.48
12363	45.2	0.7	15.32
22271	71.7	2.4	84.27
53910	132.5	4.1	628.08
87994	267.3	8.3	1024.55
158379	506.9	20.8	1638.39

Table 2 illustrates the relationship between point cloud size and model reconstruction performance. The model reconstruction time does not exhibit a linear relationship with the number of points in the point cloud. When the point cloud size is 4,651 points, reconstructing the landscape mesh model takes 2.7 milliseconds; when the point cloud size is 12,363 points, the reconstruction time is only 0.7 milliseconds; and when the point cloud size increases to 158,379 points, the reconstruction time rises to 20.8 milliseconds. At this point, computational complexity increases with data volume. However, overall, the number of model faces grows exponentially with point cloud volume. For example, when the point cloud volume is 4,651, the number of faces is 2.4817 million; when the point cloud volume is 158,379, the number of faces is 16.3839 million (a 6.6-fold increase). However, when the point cloud count is 9,125, the number of faces is only 134,800, likely due to a simple structural scene. When the point cloud count is 53,910, the number of faces reaches 6,280,800, indicating that the point cloud density of the waterwheel's main structure is high.

3.4. Comparison of Landscape Modeling Performance

Through processes such as laser point cloud data collection, feature matching optimization, and texture mapping, this paper has completed high-precision 3D modeling of the Lanzhou Waterwheel Landscape. To verify the practicality and superiority of this approach, this chapter will systematically evaluate the model's performance using experimental data and conduct a multi-dimensional comparative analysis with mainstream modeling methods.

To validate the effectiveness and practicality of the method proposed in this paper, three-dimensional models of the Lanzhou Waterwheel architectural landscape were created using four different methods: a three-dimensional model of buildings based on oblique photography from a single-lens drone (referred to as Method A), a modeling and virtual design method based on three-dimensional virtual landscapes

(referred to as Method B), a three-dimensional landscape modeling method combining oblique photography and laser scanning technology (referred to as Method C), and the method proposed in this paper. The superiority of the proposed model was validated from three aspects: modeling time, modeling accuracy, and modeling stereoscopic level.

3.4.1. Comparison of Modeling Duration

The modeling phase is divided into five segments. Table 3 shows the test results for the modeling time required for each method.

Table 3. Test results of the duration used for modeling by each method.

Modeling stage	Duration of modeling /min			
	Method A	Method B	Method C	OURS
1	8.50	6.38	5.26	3.27
2	11.97	9.30	5.07	2.09
3	13.90	11.73	8.50	3.77
4	15.70	13.96	8.81	3.21
5	11.17	8.37	9.61	2.90
Total	61.24	49.74	37.25	15.24

The method described in this paper is significantly efficient at all stages, with a total runtime of approximately 15.24 minutes. This represents reductions of 74.7%, 69.4%, and 59.1% compared to Method A (60.24 minutes), Method B (49.74 minutes), and Method C (37.25 minutes), respectively. The most significant advantages are observed in stages 2 and 4, where the time required is only 41.2% and 36.4% of that for Method C, respectively, highlighting the improved efficiency of the RANSAC algorithm and feature matching process. The proposed method takes only 2.90 minutes for model integration in stage 5, far below the 9.61 minutes for Method C, indicating that the proposed assembly correction process is more optimized.

3.4.2. Comparison of Feature Point Distance Errors

Once the efficiency advantage has been established, the geometric accuracy of the model must be verified. The ability of different methods to reproduce the detailed structure of the waterwheel is quantified using the distance error between feature points at the same location.

Seven feature points at the same location are randomly selected from the architectural landscape models constructed by each method. The distances between each feature point are measured in AutoCAD. The measurement error results for the distances between feature points for each method are shown in Table 4. Based on the geometric error values, the ability to construct the detailed structure of the model is analyzed.

Table 4. Test results of the duration used for modeling by each method (min).

Feature point	Distance measurement error value /m			
	Method A	Method B	Method C	OURS
1	7.85	5.64	4.65	2.91
2	7.01	6.80	5.43	2.01
3	7.63	8.69	6.14	2.16
4	8.13	6.73	5.24	1.61
5	5.49	7.88	7.11	2.88
6	6.86	5.40	5.40	1.36
7	5.74	5.99	4.53	3.36
Average	6.96	6.73	5.50	2.33

The mean method error of this method is 2.33 m, which is 66.5%, 65.4%, and 57.6% lower than the 6.96 m of Method A, the 6.73 m of Method B, and the 5.50 m of Method C, respectively, demonstrating significantly superior accuracy. Among all 7 feature points, the error of the method proposed in this paper is lower than that of other methods, with 6 points having errors ≤ 3 m (only point 7 is 3.36 m), while other methods generally exceed 5 m. Methods B and C exhibit significant error fluctuations at certain points, such as point 3 in Method B reaching 8.69 m, whereas the method proposed in this paper demonstrates stability with a range of only 2.0 m, validating the robustness of point cloud segmentation and feature matching optimization.

3.4.3. Comparison of Modeling Stereoscopic Levels

In addition to efficiency and accuracy, three-dimensional expressiveness is a core indicator of three-dimensional landscapes. This section uses spatial limit indicators to reveal differences in spatial realism between different methods. Figure 8 compares the three-dimensional levels of outdoor landscape models created using four different methods. A limit indicator is set in the spatial coordinate system.

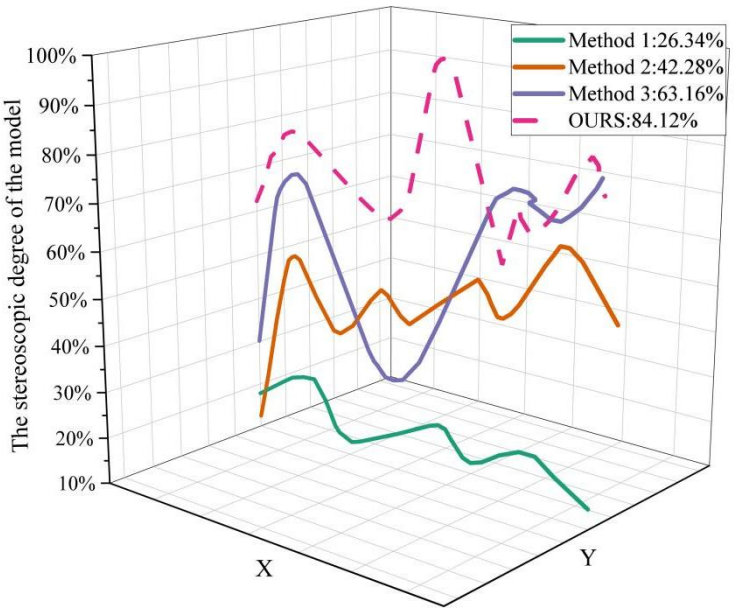

Figure 8. The 3D levels of different methods.

After testing, it was found that the model stereoscopic level of Method A, based on oblique photography using a single-lens drone, exceeded the stereoscopic level limit, resulting in an overly virtual model that could not be imaged, with a stereoscopic level of only 26.34%. The model stereoscopic level of Method B, based on three-dimensional virtual landscapes, was 42.28%, while the model stereoscopic level of Method C, which combines oblique photography with laser scanning technology, was 63.16%. The model stereoscopic level of the proposed method was 84.12%, which is relatively high without causing distortion. Therefore, it can be concluded that the proposed method achieves a high level of stereoscopic accuracy. This is because the proposed method performs data fusion processing on point cloud data before conducting three-dimensional outdoor landscape modeling, thereby reducing data volume, simplifying computational steps, enhancing modeling efficiency, and ultimately improving the stereoscopic accuracy of the model.

4. Conclusion

This study achieved high-precision digital reconstruction of the Lanzhou Waterwheel Landscape by integrating 3D laser scanning with optimization algorithms.

(1) Subjective evaluations showed that the model accuracy score reached 94.85 points, with resolution and material texture scores of 95.45 and 92.50 points, respectively, and lighting and shadow effects exceeding 93 points, confirming the high fidelity of geometric structure and visual features.

(2) The average feature point distance error was only 2.33 m, a reduction of 57.6–66.5% compared to the 5.50–6.96 m of traditional methods, highlighting the effectiveness of point cloud segmentation and matching optimization.

(3) After introducing the AKAZE algorithm, skeleton extraction time was reduced by 12.1–18.0%,

such as from 314.5 ms to 276.4 ms for a 158,379-point cloud, effectively alleviating the time consumption expansion issue in large-scale data processing.

(4) The total modeling time for the entire process was only 5.24 minutes, which is up to 74.7% faster than the 61.24 minutes for oblique photography method A and the 49.74 minutes for virtual design methods.

(5) In spatial limit tests, the model achieved a stereoscopic level of 84.12%, far exceeding the 26.34% of single-lens drones and the 63.16% of laser oblique photography fusion methods, attributed to point cloud fusion simplifying computational steps.

In summary, this method achieves significant advantages in terms of accuracy, efficiency, and realism through point cloud registration, feature matching (improved RANSAC), and texture mapping optimization.

References

1. Zhao, Z. J. (2019). Landscape Design Based on Regional Culture. In 2018 International Workshop on Advances in Social Sciences, Edited by Z. Zhu (pp. 402-405).
2. Zhao, X., & Binti Che Amat, R. (2025). Application and evaluation of traditional garden culture in modern urban landscape design under the context of cultural sustainability. PLoS One, 20(5), e0324613.
3. Zhao, D., Shang, Y., Liu, W., & Liu, G. (2019, May). Research of Regional Design Based On The Invention and Innovative Design Of The Yellow River Waterwheel's Traditional Characteristics. In 2019 2nd International Conference on Sustainable Energy, Environment and Information Engineering (SEEIE 2019) (pp. 157-161). Atlantis Press.
4. Plieninger, T., Bieling, C., Fagerholm, N., Byg, A., Hartel, T., Hurley, P., ... & Huntsinger, L. (2015). The role of cultural ecosystem services in landscape management and planning. Current Opinion in Environmental Sustainability, 14, 28-33.
5. Cortesão, J., & Lenzholzer, S. (2022). Research through design in urban and landscape design practice. Journal of Urban Design, 27(6), 617-633.
6. Misthos, L. M., Krassanakis, V., Merlemis, N., & Kesidis, A. L. (2023). Modeling the visual landscape: a review on approaches, methods and techniques. Sensors, 23(19), 8135.
7. Larsen, L. G., Eppinga, M. B., Passalacqua, P., Getz, W. M., Rose, K. A., & Liang, M. (2016). Appropriate complexity landscape modeling. Earth-science reviews, 160, 111-130.
8. Salehabadi, A. M., Ghoddusifar, S. H., & Mohammadpor, A. (2023). Analytical Model of Landscape Architecture Planning Using GIS-Based Information Systems Based on Digital Visual and Analytical Models. International Journal of Architectural Engineering & Urban Planning, 33(3).
9. Polat, A. T., & Akay, A. (2015). Relationships between the visual preferences of urban recreation area users and various landscape design elements. Urban Forestry & Urban Greening, 14(3), 573-582.
10. Vugule, K., Mengots, A., & Stokmane, I. (2018). Road landscape modelling. RESEARCH FOR RURAL DEVELOPMENT, 1.
11. Tortora, A., Statuto, D., & Picuno, P. (2015). Rural landscape planning through spatial modelling and image processing of historical maps. Land Use Policy, 42, 71-82.
12. Jamei, E., Mortimer, M., Seyedmahmoudian, M., Horan, B., & Stojcevski, A. (2017). Investigating the role of virtual reality in planning for sustainable smart cities. Sustainability, 9(11), 2006.
13. Lovett, A., Appleton, K., Warren-Kretzschmar, B., & Von Haaren, C. (2015). Using 3D visualization methods in landscape planning: An evaluation of options and practical issues. Landscape and Urban Planning, 142, 85-94.
14. Yang, Z. H. A. N. G., Changlin, L. I., & Fei, W. U. (2021). Interactive Landscape Practice and Future Trends Driven by Digital Technology. Landscape Architecture, 28(4), 99-104.
15. Shi, B. (2024). 3D dynamic landscape simulation of artificial intelligence in environmental landscape design. Heliyon, 10(15).
16. Yang, S., & Yang, J. (2020). Design of urban landscape visual simulation system based on three-dimensional simulation technology. International Journal of Industrial and Systems Engineering, 36(2), 266-280.
17. Zhao, X. (2020). Application of 3D CAD in landscape architecture design and optimization of hierarchical details. Computer-Aided Design and Applications, 18(S1), 120-132.
18. Li, R., & Xu, D. (2020). Distribution of landscape architecture based on 3D images and virtual reality rationality study. IEEE access, 8, 140161-140170.
19. Liu, M., & Nijhuis, S. (2020). Mapping landscape spaces: Methods for understanding spatial-visual characteristics in landscape design. Environmental Impact Assessment Review, 82, 106376.
20. Piga, B., & Morello, E. (2015). Environmental design studies on perception and simulation: an urban design approach. Ambiances. Environnement sensible, architecture et espace urbain, (1).
21. Jun, Y., & Xian, S. X. (2020, November). Research on landscape design based on digital technology. In Journal of Physics: Conference Series (Vol. 1651, No. 1, p. 012071). IOP Publishing.
22. Tian, Z. (2022). Application of computer 3D modeling technology in the simulation design of modern garden ecological landscape. Mathematical problems in engineering, 2022(1), 7033261.
23. Liu, C., Lin, M., Rauf, H. L., & Shareef, S. S. (2021). Parameter simulation of multidimensional urban landscape design based on nonlinear theory. Nonlinear Engineering, 10(1), 583-591.

24. Liu, X. (2020). Three-dimensional visualized urban landscape planning and design based on virtual reality technology. IEEE access, 8, 149510-149521.
25. Lee, M. J. (2018). Functions and roles of digital landscape architectural drawing. Journal of the Korean Institute of Landscape Architecture, 46(2), 1-13.
26. Shan, P., & Sun, W. (2021). Research on landscape design system based on 3D virtual reality and image processing technology. Ecological Informatics, 63, 101287.